Accelerating slow excited state proton transfer

David J. Stewart, Javier J. Concepcion, M. Kyle Brennaman, Robert A. Binstead, and Thomas J. Meyer[1]

Department of Chemistry, University of North Carolina, Chapel Hill, NC 27599

Visible light excitation of the ligand-bridged assembly $[(bpy)_2Ru_a^{II}(L)$ $Ru_b^{II}(bpy)(OH_2)^{4+}]$ (bpy is 2,2′-bipyridine; L is the bridging ligand, 4-phen-tpy) results in emission from the lowest energy, bridge-based metal-to-ligand charge transfer excited state $(L^{-•})Ru^{III}\text{-}OH_2$ with an excited-state lifetime of 13 ± 1 ns. Near–diffusion-controlled quenching of the emission occurs with added HPO_4^{2-} and partial quenching by added acetate anion (OAc^-) in buffered solutions with pH control. A Stern–Volmer analysis of quenching by OAc^- gave a quenching rate constant of $k_q = 4.1 \times 10^8$ $M^{-1}\cdot s^{-1}$ and an estimated pK_a^* value of $\sim 5 \pm 1$ for the $[(bpy)_2Ru_a^{II}(L^{•-})Ru_b^{III}(bpy)$ $(OH_2)^{4+}]^*$ excited state. Following proton loss and rapid excited-state decay to give $[(bpy)_2Ru_a^{II}(L)Ru_b^{II}(bpy)(OH)^{3+}]$ in a $H_2PO_4^-/$ HPO_4^{2-} buffer, back proton transfer occurs from $H_2PO_4^-$ to give $[(bpy)_2Ru_a^{II}(L)Ru_b(bpy)(OH_2)^{4+}]$ with $k_{PT,2} = 4.4 \times 10^8$ $M^{-1}\cdot s^{-1}$. From the intercept of a plot of k_{obs} vs. $[H_2PO_4^-]$, $k = 2.1 \times 10^6$ s^{-1} for re-protonation by water providing a dramatic illustration of kinetically limiting, slow proton transfer for acids and bases with pK_a values intermediate between $pK_a(H_3O^+) = -1.74$ and $pK_a(H_2O) = 15.7$.

kinetics | photochemistry | luminescence | transient absorption

Proton transfer (1–5) and proton-coupled electron transfer (6–14), with proton gain or loss triggered by changes in electron content, are ubiquitous in chemistry and biology. The gain or loss of protons in water tied to oxidation or reduction is generally assumed to be rapid and not rate limiting. However, water is a weak proton acceptor with $pK_a(H_3O^+) = -1.74$ and a weak proton donor with $pK_a(H_2O) = 15.7$. For acids and bases having intermediate pK_a values, this creates a kinetic inhibition to proton transfer to or from the solvent. Following Krishtalik (4, 15) and the experimental observations of Nibbering and coworkers (16–18) and Scandola and coworkers (19) and the detailed analysis of Agmon (20), acid dissociation from a generalized acid HA can be partitioned into two steps: initial proton dissociation with proton transfer to a water molecule or cluster (Eq. 1*A*), followed by dilution in the surrounding medium (Eq. 1*B*). Except for very strong acids, proton dissociation is nonspontaneous with $\Delta G_{diss}(eV) \sim$ $-0.059[pK_a(H_3O^+) - pK_a(HA)]$. The final equilibrium state following dissociation is defined by the acid dissociation constant and the prevailing conditions—temperature, ionic strength, etc. Similarly, proton transfer from the solvent to an added base, B, occurs by initial proton transfer to the base followed by dilution.
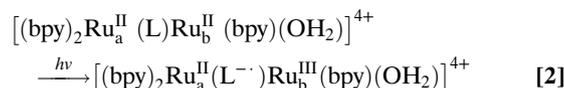
$$AH\text{---}OH_2 \rightarrow A^-\text{---}H\text{-}OH_2^+ \qquad [1A]$$

$$A^-\text{---}H\text{-}OH_2^+ \rightarrow A^- + H_3O^+ \text{ (pH)} \qquad [1B]$$

Proton loss to solvent in Eq. 1*A* can be considerably disfavored for acids having pK_a values intermediate between H_3O^+ and H_2O with ΔG_{diss} of ~ 0.52 eV for an acid with $pK_a = 7$. The magnitude of ΔG_{diss} also sets the minimum activation barrier for the initial proton transfer step. Microscopically, proton transfer from HA occurs to an initially H-bonded water molecule or water cluster (21). Given the high frequency of the O-H vibrational modes for proton transfer, at or near room temperature, the proton transfer steps are inherently quantum mechanical with rapid rates relying on preassociation to minimize the proton transfer distance and maximize vibrational wave function overlap (22–24).

These considerations are especially important for short-lived intermediates and excited states. For excited states, changes in pK_a are induced by the change in electronic configuration in the excited state and can be considerable as evidenced by the enhanced acidities of excited-state "super acids" (20, 25–31). With limited lifetimes, barriers to proton dissociation are often too high to allow the excited state to reach acid–base equilibrium, $HA^* + H_2O = A^{-*} + H_3O^+$.

We report here the results of a photophysical study designed to investigate the dynamic impact of slow proton transfer of excited states in water including the observation and exploitation of catalyzed proton loss by added bases. Related experimental observations have been reported by Gryczynski and coworkers (32, 33) based on protonation of pyrene-1-carboxylate in the presence of a phosphate buffer and by Alvarez-Pez et al. (34, 35) on fluorescence from fluorescein also with added phosphate buffers.

Our observations were made on a short-lived metal-to-ligand charge transfer (MLCT), assembly-based excited state of the complex $[(bpy)_2Ru_a^{II}(L^{•-})Ru_b^{III}(bpy)(OH_2)^{4+}]$ (1, bpy is 2,2′-bipyridine; L is the bridging ligand, 4-phen-tpy) (see Fig. 2). For related aqua-based complexes, significant changes in pK_a are observed in the ground states between $Ru^{II}\text{-}OH_2$ and $Ru^{III}\text{-}OH_2$ with a decrease in pK_{a1} from 10.8 for $Ru^{II}(bpy)_2(py)(OH_2)^{2+}$ to 0.85 for $Ru^{III}(bpy)_2(py)(OH_2)^{3+}$ (py is pyridine) (36). From pH-dependent electrochemical and UV-vis absorption data, the pK_a for $[(bpy)_2Ru_a^{II}(L)Ru_b^{III}(bpy)(OH_2)^{5+}]$ is <1.0, and for $[(bpy)_2Ru_a^{II}(L)Ru_b^{II}(bpy)(OH_2)^{4+}]$, it is 9.57 ± 0.05 (Fig. S1).

In 1 (structure in Fig. 1), the lowest energy absorption in the visible (Fig. 1) arises from an internal charge transfer to the bridging ligand (Eq. 2) to give the excited state $[(bpy)_2Ru_a(L^{-•})$ $Ru_b^{III}(bpy)(OH_2)]^{4+*}$ (1*). In these molecules, light absorption is dominated by MLCT transitions to excited states largely singlet in character followed by rapid internal conversion and decay to the corresponding, lowest energy "triplet" states, which are observed spectroscopically (37, 38). In 1*, the lowest MLCT excited state is $(L^{-•})Ru_b^{III}\text{-}OH_2$ with the assignment supported by time-dependent density functional theory (TD-DFT) (Fig. S2). A pK_a intermediate between $Ru^{II}\text{-}OH_2$ and $Ru^{III}\text{-}OH_2$ is expected for this $^3(d\pi_{Rub}^5 \pi^*_L)$, $(L^{-•})Ru_b^{III}\text{-}OH_2$ excited state.

$$[(bpy)_2Ru_a^{II}(L)Ru_b^{II}(bpy)(OH_2)]^{4+}$$
$$\xrightarrow{hv} [(bpy)_2Ru_a^{II}(L^{-•})Ru_b^{III}(bpy)(OH_2)]^{4+} \qquad [2]$$

Results and Discussion

Excited-State Properties. Absorption spectra for 1, in water as $\text{-}Ru^{II}\text{-}OH_2$, and in 0.1 M NaOH, as $\text{-}Ru^{II}\text{-}OH$ in $[(bpy)_2Ru_a^{II}(L)$ $Ru_b^{II}(bpy)(OH)]^{3+}$ (2) (Fig. 1), are dominated by intense, ligand-localized $\pi \rightarrow \pi^*$ bands in the UV and the characteristic

Fig. 1. Chemical structure and absorption spectra of **1** in water (black) and 0.1 M NaOH (red).

MLCT bands in the visible. In the visible spectrum in water, a broad absorption is observed from 400 to 550 nm with λ_{max} of ~470 nm arising from overlapping $d\pi(Ru_a) \rightarrow \pi^*(bpy),\pi^*(L)$ and $d\pi(Ru_b) \rightarrow \pi^*(tpy),\pi^*(L)$ MLCT absorptions. Deprotonation in 0.1 M NaOH results in a distinct MLCT absorption at $\lambda_{max} = 452$ nm, largely due to MLCT absorptions at Ru^{II}_a, and a lower energy absorption at λ_{max} of ~525 nm, largely originating at $-Ru^{II}_b$-OH. As mentioned above, these assignments are all supported by TD-DFT calculations (Fig. S2).

In normalized emission spectra of **1** in water at varying excitation wavelengths, two distinct MLCT emissions are observed (Fig. S3A). One, attributable to $Ru^{III}_a(L^{\bullet-})$, appears as a high-energy shoulder at ~625 nm [compared with 620 nm for Ru(bpy)$_3^{2+*}$ under the same conditions]. The other, at 755 nm, is attributable to emission from $^3[(bpy)_2Ru^{II}(L^{\bullet-})Ru^{III}(bpy)(OH_2)_2^{4+}]^*$ with the electron localized on the bridging ligand. No emission was observed from **2**, and there was no evidence for **2*** in transient emission and absorption measurements on the 10-ns timescale (see below). Based on the excitation dependence, the 755-nm emission arises both from direct excitation and by excitation of the $Ru^{II}_a \rightarrow bpy,L$ chromophores followed by rapid internal conversion and intraassembly energy transfer. The latter was too rapid to monitor on the timescale (~10 ns) of our measurements. The emitting $(L^{\bullet-})Ru^{II}_b$-OH$_2$–based excited state has a lifetime of 13 ± 1 ns in water by transient absorption and emission measurements (Fig. S3B).

Time-dependent transient absorption (TA) difference spectra for **1*** are shown in Fig. S3C. The first spectrum was obtained ~18 ns after excitation at 460 nm and is consistent with formation of $(L^{\bullet-})Ru^{III}_b$-OH$_2$. It features a bleach centered at 495 nm and a broad, positive absorption feature in the low energy visible/near-infrared spectrum from 580 to 800 nm. The latter is typical for $\pi \rightarrow \pi^*$ absorptions of reduced polypyridine ligands (39) with a contribution from ligand-to-metal charge transfer (40) at Ru(III). Excited-state decay kinetics were independent of monitoring

Fig. 3. Calculated (black) and experimental (red) transient absorption difference spectra for **1**. The calculated spectrum was obtained by subtracting the ground state spectrum in pure water from the spectrum in 0.1 M NaOH. The experimental spectrum was acquired by CCD camera detection 18 ns after laser flash excitation at 460 nm: [**1**] = 21.2 μM, [NaOAc] = 50 mM, [HOAc] = 5.1 mM, μ = 0.5 M (NaOOCCF$_3$), pH = 5.42.

wavelength and match those observed by emission with $\tau = 13 \pm 1$ ns. The transient results are consistent with Fig. 2.

Influence of Added Bases. Addition of acetate buffer [[HOAc] = 5.1 mM; [OAc$^-$] = 50 mM; pH = 5.42; μ = 0.5 M (NaOOCCF$_3$)], results in a new, positive absorption feature in the TA difference spectrum at 565 nm, with the bleach at 495 nm relatively unaffected. The transient difference spectrum is essentially identical to a spectrum calculated by subtracting the absorption spectrum in water from the spectrum in 0.1 M NaOH (Fig. 3). This observation is consistent with excitation of **1** and relaxation to give $(L^{\bullet-})Ru^{III}_b$-OH$_2$ followed by rapid deprotonation by the added base to give **2** (Fig. 4).

The effects of added buffer bases on the excited-state dynamics were examined by adding increasing amounts of the added sodium salts of acetate (OAc$^-$), HPO$_4^{2-}$, or H$_2$PO$_4^-$ with control of pH by addition of the conjugate acids. The effects observed were buffer base dependent and not due to pH variations. This was shown by a series of experiments in which the base concentration was held constant and conjugate acid varied to change the pH. Emission spectra with added buffer bases are shown in Figs. 5 and 6 and Fig. S4.

For the strongest base, HPO$_4^{2-}$ with pK$_a$(H$_2$PO$_4^-$) = 7.2, significant excited-state quenching occurred as [HPO$_4^{2-}$] was increased, as observed by both steady-state (Fig. 5) and time-resolved emission measurements (Fig. S5A). As shown by the data in Fig. 5, ~50% quenching was reached with 100 mM added HPO$_4^{2-}$. A Stern–Volmer analysis of the data as $1/\tau = 1/\tau_o + k_q[HPO_4^{2-}]$, with τ and τ_o the lifetimes with and without added buffer base, respectively, gave $k_{q,obs} = 1.2 \times 10^9$ M$^{-1}\cdot$s^{-1} (Fig. 7).

Fig. 2. Excitation–decay sequence for **1*** in water on the nanosecond timescale.

Fig. 4. Mechanism for excited-state deprotonation and relaxation with added acetate anion.

Fig. 5. Emission spectra of **1*** in water with varying [Na$_2$HPO$_4$]. [**1**] = 18.3 μM, [NaH$_2$PO$_4$] = 60 mM, μ = 0.5 M (NaOOCCF$_3$), λ$_{ex}$ = 530 nm.

Fig. 7. Variation in the rate constant for excited-state emission decay (k_{obs}) vs. [Base]. [**1**] = 18.3 μM, [conjugate acid] = 60 mM, μ = 0.5 M (NaOOCCF$_3$), λ$_{ex}$ = 484 nm, λ$_{det}$ = 760 nm.

This value is uncorrected for diffusional effects with, $1/k_{q,obs} = 1/k_D + 1/k_q$, and k_D the diffusion-limited rate constant.

Acetate (pK$_a$ = 4.8) is a weaker base than HPO$_4^{2-}$ by 2.4 pK$_a$ units. With 100 mM added OAc$^-$ at pH = 4.84, **1*** is only ~20% quenched. Stern–Volmer analysis of the dependence of the emission lifetime on [OAc$^-$] gave $k_q = 4.1 \times 10^8$ M^{-1}·s^{-1} (Fig. 7), well below the diffusion-controlled limit. With added H$_3$PO$_4$/H$_2$PO$_4^-$ [pK$_a$(H$_3$PO$_4$) = 2.2], there was no sign of emission quenching by either steady-state or time-resolved measurements up to [H$_2$PO$_4^-$] = 200 mM (Fig. S4).

Quenching Mechanism. The observations made here are consistent with the quenching mechanism in Fig. 4. In this mechanism, MLCT excitation and excited state and energy transfer equilibration occur in a preformed, ion pair/H-bonded association complex between the coordinated -OH$_2$ ligand at [(L$^{•-}$)Ru^{III}$_b$-OH$_2$]$^{4+}$ and added OAc$^-$. Preassociation and H bonding are required for proton transfer to OAc$^-$ to occur given the short excited-state lifetime. In the association complex, proton transfer to the base leads to the deprotonated excited state, ^{3}[(bpy)$_2$Ru^{II}(L$^{•-}$) Ru^{III}(bpy)(OH)$^{3+}$]*. It undergoes rapid nonradiative decay to the ground state as shown by transient absorption measurements on

[(bpy)$_2$Ru^{II}(L)Ru^{II}(bpy)(OH)]$^{3+}$*, which, following MLCT excitation, showed no evidence for a transient on the ~10-ns timescale.

The experimentally observed quenching rate constant for OAc$^-$ as the added base was $k_q = 4.1 \times 10^8$ M^{-1}·s^{-1}. From the mechanism in Fig. 4, $k_q = K_A k^*_{PT}$ with K_A, the association/ion pair constant, and k^*_{PT}, the rate constant for excited-state proton transfer. The quenching results do not provide direct information about the excited-state pK$_a$, only that deprotonation of the excited state has occurred. In the classical limit, the proton transfer barrier is given by $\Delta G^* = \lambda/4(1 + \Delta G^{o\prime}/\lambda)^2 \sim \lambda/4 + \Delta G^{o\prime}/2$ ($\Delta G^{o\prime} < \lambda$), with $\Delta G^{o\prime}$ the driving force for proton transfer and λ the reorganization energy (41–43). As noted above, $\Delta G^{o\prime}$ is the minimum barrier for proton transfer to occur ($\lambda = 0$), which, in this case, is given by $\Delta G^{o\prime}$(eV) $\sim -0.059[$pK$_a$(HOAc) $-$ pK$_{a,1}$*(^{3}(L$^{•-}$) Ru^{III}-OH$_2$)]. In the absence of detailed information about the reorganization energy, given the quenching data for the three bases with values of pK$_a$ = 2.2, 4.8, and 7.2, and slow, apparently partial proton transfer to OAc$^-$, we estimate that pK$_{a,1}$* ~ 5 ± 1 for the excited state.

There is independent evidence for the preassociation complex in the emission data with added OAc$^-$ in Fig. 4. It appears in the

Fig. 6. Emission spectra for **1*** in water at room temperature with varying [NaOAc]. [**1**] = 19.2 μM, [HOAc] = 60 mM, μ = 0.5 M (NaOOCCF$_3$), λ$_{ex}$ = 530 nm.

Fig. 8. Time-resolved transient absorption traces for **1** in water at room temperature with varying [Na$_2$HPO$_4$]. [**1**] = 18.3 μM, [NaH$_2$PO$_4$] = 60 mM, μ = 0.5 M (NaOOCCF$_3$), λ$_{ex}$ = 460 nm and absorption monitoring at 565 nm.

Stewart et al.

Fig. 9. Transient absorption difference spectra of **1** in water with [Na₂HPO₄] = 20 mM (black) and 100 mM (red). Measured 28 ns after the laser pulse, [**1**] = 18.3 μM, [NaH₂PO₄] = 60 mM, μ = 0.5 M (NaOOCCF₃), λ_{ex} = 460 nm.

red shift of ∼20 nm in the emission maximum as [OAc⁻] was increased from 0 to 100 mM (Fig. 6). There was no evidence of a similar effect with added HPO_4^{2-} (Fig. 5) for which quenching is near the diffusion-controlled limit. For OAc⁻, the importance of the proton transfer step in quenching is shown by the observation of a H₂O/D₂O kinetic isotope effect (KIE) of 2.6 (Fig. S6A). By contrast, with HPO_4^{2-} as the added base, KIE ∼ 1.3 (Fig. S6B).

Reprotonation: Slow Proton Transfer. Excited-state deprotonation is rapid and irreversible with no sign of reprotonation and equilibrium with the deprotonated excited state even at high concentrations of added buffer acid. Once ground state [(bpy)₂Ru^II(L)Ru^II(bpy)(OH)]³⁺ is formed, it is possible to monitor its reprotonation kinetics by transient absorption measurements. Absorbance–time traces are shown in Fig. 8 as a function of added [HPO_4^{2-}] at constant [$H_2PO_4^-$]. The amplitude of the absorbance change at 565 nm (ΔOD) increases with added HPO_4^{2-} consistent with increased formation of **2** during the laser pulse; note the relative amplitude changes for 20 and 100 mM HPO_4^{2-} in Fig. 9 with nearly complete formation of **2** for the latter. The subsequent reprotonation kinetics was independent of the concentration of the base form of the buffer and of the solution pH (Fig. S7A).

Quenching of the excited state is independent of the acid form of the buffer (Fig. S5B), but the reprotonation kinetics does depend on the acid form. This was demonstrated in a series of experiments in which [HPO_4^{2-}] was held constant while varying [$H_2PO_4^-$]. In these experiments, with [HPO_4^{2-}] = 60 mM, the same amount of **2** was formed following laser flash excitation in the series of experiments. Monitoring the transient absorption decay kinetics at 565 nm (Fig. 10) shows that the kinetics of return of **2** to **1** are first order in [$H_2PO_4^-$]. From the slope of the plot of k_{obs} vs. [$H_2PO_4^-$], $k_{PT,2}$ = 4.4 × 10⁸ M⁻¹·s⁻¹ in water. Based on a parallel study in D₂O, KIE = 1.3 (Fig. S7B).

From the intercept of the plot of k_{obs} vs. [$H_2PO_4^-$], the rate constant for reprotonation of **1** is 2.1 × 10⁶ s⁻¹ in water with water as the proton donor (Eq. 3). This value provides a dramatic illustration of the kinetic inhibition to proton gain or loss by water for acids and bases with pKa values intermediate between $pK_a(H_3O^+)$ = −1.74 and $pK_a(H_2O)$ = 15.7. As noted above, the origin of the inhibition is the energetically unfavorable initial

proton transfer step from a water molecule or cluster, [(bpy)₂Ru^II(L)Ru^II(bpy)-O(H)—H₂O_aq]³⁺ → ([(bpy)₂Ru^II(L)Ru^II(bpy)-O(H)-H]⁴⁺—OH⁻_aq)³⁺ with ΔG°′(eV) ∼ −0.059(pK_a(-Ru^II-OH₂) − pK_a(H₂O) ∼ + 0.6 eV.

$$[(bpy)_2\,Ru^{II}\,(L)Ru^{II}\,(bpy)\text{-}OH]^{3+}\;+\;H_2O$$
$$\rightarrow [(bpy)_2Ru^{II}(L)Ru^{II}(bpy)\text{-}OH_2]^{4+} + OH^- \qquad [3]$$

$$OH^-\;+\;HOAc\;=\;H_2O\;+\;OAc^-$$
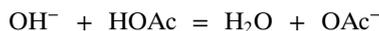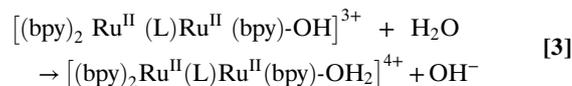
Our photophysical results on the lowest, bridge-based MLCT excited state in the assembly [(bpy)₂Ru_a^II(L)Ru_b^II(bpy)(OH₂)]⁴⁺ (bpy is 2,2′-bipyridine; L is the bridging ligand, 4-phen-tpy) illustrate the importance of a kinetic inhibition to proton transfer for acids and bases in water with pKa values intermediate between H₃O⁺ and H₂O. For short-lived excited states, proton transfer can still occur by preassociation of a proton acceptor base with proton transfer giving the conjugate base of the excited state. Based on the results of a kinetic analysis of emission lifetime data in acetate/acetic acid buffer solutions, pK_a* ∼ 5 ± 1 for the [(bpy)₂Ru_a^II(L•⁻)Ru_b^III(bpy)(OH₂)⁴⁺]* MLCT excited state. Following deprotonation of the excited state to give [(bpy)₂Ru^II(L)Ru^II(bpy)-OH]³⁺ in $H_2PO_4^-$/HPO_4^{2-} buffer solutions, the photochemically prepared base [(bpy)₂Ru^II(L)Ru^II(bpy)-OH]³⁺ undergoes reprotonation with $H_2PO_4^-$ with $k_{PT,2}$ = 4.4 × 10⁸ M⁻¹·s⁻¹ and, by extrapolation, with water with k = 2.1 × 10⁶ s⁻¹. The latter illustrates a profound kinetic inhibition to proton transfer.

Materials and Methods

Detailed synthesis, characterization, synthetic scheme, instrumentation, experimental methods, and supplementary figures are located in SI Text. The detailed synthetic scheme is given in Fig. S8. Characterization of the final product includes cyclic and square wave voltammetry (Fig. S9) as well as NMR (Fig. S10). NMR spectra are included for the intermediates as well. The SI Text also gives detailed information on the DFT calculations and the spectrophotometric titration used to determine the ground state pKa.
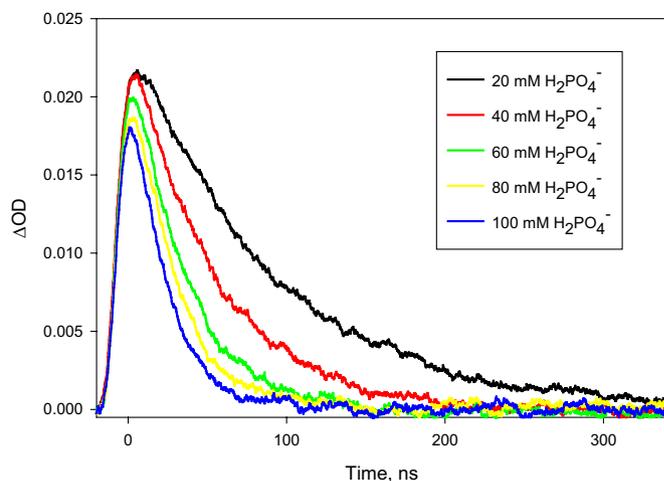
Fig. 10. Time-resolved absorption decay of **1** in water with varying [$H_2PO_4^-$]. [**1**] = 20.7 μM, [HPO_4^-] = 60 mM, μ = 0.5 M (NaOOCCF₃), λ_{ex} = 460 nm, λ_{det} = 565 nm.

CHEMISTRY

1. Eigen M (1963) Proton transfer, acid-base catalysis, and enzymic hydrolysis. I. Elementary processes. *Angew Chem Int Ed Engl* 75(12):489–508.
2. Eigen M, Kruse W, Maass G, de Maeyer L (1964) Rate constants of protolytic reactions in aqueous solution. *Progr Reaction Kin* 2:285–318.
3. Weller A (1956) Intramolecular proton transfer in excited states. *Z Elektrochem Angew Phys Chem* 60:1144–1147.
4. Krishtalik LI (2000) The mechanism of the proton transfer: An outline. *Biochim Biophys Acta. Bioenerg* 1458(1):6–27.
5. Marx D (2006) Proton transfer 200 years after von Grotthuss: Insights from ab initio simulations. *ChemPhysChem* 7(9):1848–1870.
6. Huynh MHV, Meyer TJ (2007) Proton-coupled electron transfer. *Chem Rev* 107(11):5004–5064.
7. Belevich I, Verkhovsky MI, Wikström M (2006) Proton-coupled electron transfer drives the proton pump of cytochrome c oxidase. *Nature* 440(7085):829–832.
8. Cukier RI, Nocera DG (1998) Proton-coupled electron transfer. *Annu Rev Phys Chem* 49:337–369.
9. Hammes-Schiffer S (2009) Theory of proton-coupled electron transfer in energy conversion processes. *Acc Chem Res* 42(12):1881–1889.
10. Hammes-Schiffer S (2001) Theoretical perspectives on proton-coupled electron transfer reactions. *Acc Chem Res* 34(4):273–281.
11. Mayer JM (2004) Proton-coupled electron transfer: A reaction chemist's view. *Annu Rev Phys Chem* 55:363–390.
12. Meyer TJ, Huynh MHV, Thorp HH (2007) The possible role of proton-coupled electron transfer (PCET) in water oxidation by photosystem II. *Angew Chem Int Ed Engl* 46(28):5284–5304.
13. Reece SY, Hodgkiss JM, Stubbe J, Nocera DG (2006) Proton-coupled electron transfer: The mechanistic underpinning for radical transport and catalysis in biology. *Philos Trans R Soc Lond B Biol Sci* 361(1472):1351–1364.
14. Rhile IJ, et al. (2006) Concerted proton-electron transfer in the oxidation of hydrogen-bonded phenols. *J Am Chem Soc* 128(18):6075–6088.
15. Krishtalik LI (1982) Proton transfer in electrode reactions. Experimental test of two theoretical models. *Faraday Discuss Chem Soc* 74:205–213.
16. Mohammed OF, Pines D, Dreyer J, Pines E, Nibbering ETJ (2005) Sequential proton transfer through water bridges in acid-base reactions. *Science* 310(5745):83–86.
17. Rini M, Magnes B-Z, Pines E, Nibbering ETJ (2003) Real-time observation of bimodal proton transfer in acid-base pairs in water. *Science* 301(19):349–352.
18. Rini M, Pines D, Magnes B-Z, Pines E, Nibbering ETJ (2004) Bimodal proton transfer in acid-base reactions in water. *J Chem Phys* 121(19):9593–9610.
19. Davila J, Bignozzi CA, Scandola F (1989) Excited-state proton-transfer processes of cis-dicyanobis(2,2'-bipyridine)ruthenium(II) in acetonitrile/water solvent systems. *J Phys Chem* 93(4):1373–1380.
20. Agmon N (2005) Elementary steps in excited-state proton transfer. *J Phys Chem A* 109(1):13–35.
21. Marx D, Tuckerman ME, Hutter J, Parrinello M (1999) The nature of the hydrated excess proton in water. *Nature* 397(6720):601–604.
22. Hammes-Schiffer S, Tully JC (1994) Proton transfer in solution: Molecular dynamics with quantum transitions. *J Chem Phys* 101(6):4657–4667.
23. Staib A, Borgis D, Hynes JT (1995) Proton transfer in hydrogen-bonded acid-base complexes in polar solvents. *J Chem Phys* 102(6):2487–2505.
24. Douhal A, Lahmani F, Zewail AH (1996) Proton-transfer reaction dynamics. *Chem Phys* 207(2–3):477–498.
25. Arnaut LG, Formosinho SJ (1993) Excited-state proton transfer reactions. I. Fundamentals and intermolecular reactions. *J Photochem Photobiol A* 75(1):1–20.
26. Formosinho SJ, Arnaut LG (1993) Excited-state proton transfer reactions. II. Intramolecular reactions. *J Photochem Photobiol A* 75(1):21–48.
27. Tolbert LM, Haubrich JE (1994) Photoexcited proton transfer from enhanced photoacids. *J Am Chem Soc* 116(23):10593–10600.
28. Solntsev KM, Huppert D, Agmon N, Tolbert LM (2000) Photochemistry of "super" photoacids. 2. Excited-state proton transfer in methanol/water mixtures. *J Phys Chem A* 104(19):4658–4669.
29. Tolbert LM, Solntsev KM (2002) Excited-state proton transfer: From constrained systems to "super" photoacids to superfast proton transfer. *Acc Chem Res* 35(1):19–27.
30. Erez Y, Huppert D (2010) Excited-state intermolecular proton transfer of the firefly's chromophore D-luciferin. *J Phys Chem A* 114(31):8075–8082.
31. Genosar L, Cohen B, Huppert D (2000) Ultrafast direct photoacid-base reaction. *J Phys Chem A* 104(29):6689–6698.
32. Zelent B, Vanderkooi JM, Coleman RG, Gryczynski I, Gryczynski Z (2006) Protonation of excited state pyrene-1-carboxylate by phosphate and organic acids in aqueous solution studied by fluorescence spectroscopy. *Biophys J* 91(10):3864–3871.
33. Zelent B, Vanderkooi JM, Nucci NV, Gryczynski I, Gryczynski Z (2009) Phosphate assisted proton transfer in water and sugar glasses: A study using fluorescence of pyrene-1-carboxylate and IR spectroscopy. *J Fluoresc* 19(1):21–31.
34. Alvarez-Pez JM, Ballesteros L, Talavera E, Yguerabide J (2001) Fluorescein excited-state proton exchange reactions: Nanosecond emission kinetics and correlation with steady-state fluorescence intensity. *J Phys Chem A* 105(26):6320–6332.
35. Paredes JM, Crovetto L, Orte A, Alvarez-Pez JM, Talavera EM (2011) Influence of the solvent on the ground- and excited-state buffer-mediated proton-transfer reactions of a xanthenic dye. *Phys Chem Chem Phys* 13(4):1685–1694.
36. Moyer BA, Meyer TJ (1978) Oxobis(2,2'-bipyridine)pyridineruthenium(IV) ion, $[(bpy)_2(py)Ru:O]^{2+}$. *J Am Chem Soc* 100(11):3601–3603.
37. Damrauer NH, et al. (1997) Femtosecond dynamics of excited-state evolution in [Ru(bpy)_3]^{2+}. *Science* 275(5296):54–57.
38. Juris A, et al. (1988) Ruthenium(II) polypyridine complexes: Photophysics, photochemistry, electrochemistry, and chemiluminescence. *Coord Chem Rev* 84:85–277.
39. Heath GA, Yellowlees LJ, Braterman PS (1981) Spectro-electrochemical studies on tris-bipyridyl ruthenium complexes; ultra-violet, visible, and near-infrared spectra of the series [Ru(bipyridyl)_3]^{2+/1+/0/1}. *J Chem Soc Chem Commun* 6:287–289.
40. Nazeeruddin MK, Zakeeruddin SM, Kalyanasundaram K (1993) Enhanced intensities of the ligand-to-metal charge-transfer transitions in ruthenium(III) and osmium(III) complexes of substituted bipyridines. *J Phys Chem* 97(38):9607–9612.
41. Kiefer PM, Hynes JT (2002) Nonlinear free energy relations for adiabatic proton transfer reactions in a polar environment. II. Inclusion of the hydrogen bond vibration. *J Phys Chem A* 106(9):1850–1861.
42. Kiefer PM, Hynes JT (2002) Nonlinear free energy relations for adiabatic proton transfer reactions in a polar environment. I. Fixed proton donor-acceptor separation. *J Phys Chem A* 106(9):1834–1849.
43. Marcus RA (1968) Theoretical relations among rate constants, barriers, and Broensted slopes of chemical reactions. *J Phys Chem* 72(3):891–899.